SUPPLEMENTARY MATERIAL

A microfluidic-based hydrodynamic trap: Design and implementation†

Melikhan Tanyeri,[a] **Mikhil Ranka,**[a] **Natawan Sittipolkul**[a] **and Charles M. Schroeder**[*a,b]

[a]*Department of Chemical and Biomolecular Engineering, University of Illinois Urbana-Champaign, Urbana, Illinois 61801*
[b]*Center for Biophysics and Computational Biology, University of Illinois Urbana-Champaign, Urbana, Illinois 61801*

Flow in a rectangular channel

The Navier-Stokes equation and the associated boundary conditions for a pressure-driven, steady-state flow in a microchannel with a rectangular cross section is given by[1]:

$$\left(\frac{\partial^2}{\partial x^2} + \frac{\partial^2}{\partial y^2}\right)\mathbf{u} = -\frac{\Delta p}{\eta L}, \quad \text{for} \quad -\frac{w}{2} < y < \frac{w}{2} \quad \text{and} \quad 0 < z < h$$

$$\mathbf{u} = 0, \quad \text{at the boundary, i.e.} \quad y = \pm\frac{w}{2}, \quad z = 0, \quad z = h$$

where $\mathbf{u}$: velocity,
Δp: pressure difference,
η: viscosity,
w, h, L: width, height and length of the channel respectively,
x, y, z are the coordinate axes along the channel length, width and height respectively.

The solution for the velocity along the channel width (y) and height (z) is given by a Fourier series expansion:

$$\mathbf{u}(y,z) = \frac{4h^2\Delta p}{\pi^3\eta L} \sum_{n,odd}^{\infty} \frac{1}{n^3}\left[1 - \frac{\cosh\left(n\pi\frac{y}{h}\right)}{\cosh\left(n\pi\frac{w}{2h}\right)}\right]\sin\left(n\pi\frac{z}{h}\right) \qquad (S1)$$

Fig. S1 shows the velocity profile (shown in (a)) and the contours of the velocity along the channel width and height (shown in (b) and (c) respectively). The flow rate Q can be found by integrating $\mathbf{u}(y,z)$ along these axes:

$$Q = 2\int_0^{w/2} dy \int_0^h dz\, \mathbf{u}(y,z) = \frac{h^4\Delta p}{12\eta L\alpha}\left[1 - \sum_{n,odd}^{\infty} \frac{192\alpha}{(n\pi)^5}\tanh\left(\frac{n\pi}{2\alpha}\right)\right] \qquad (S2)$$

where ($\alpha = h/w$) is the aspect ratio of the channel. For channels with low aspect ratio ($\alpha \to 0$), the flow rate (Q) can be approximated by:

$$Q \approx \frac{h^4\Delta p}{12\eta L\alpha}(1 - 0.63\alpha), \qquad \text{for} \ \alpha \to 0 \qquad (S3)$$

Eq. (S3) represents a good approximation to Eq. (S2) for flow rate estimates in rectangular microchannels with low aspect ratio. For example, the error is 12.3% for $h = w$ (square channel cross-section, $\alpha = 1$), 0.15% for ($\alpha = 0.5$) and only 0.003% for ($\alpha = 0.1$). Using Eq. (S3), the flow resistance of a rectangular microchannel is approximated by:

$$R = \frac{\Delta p}{Q} \approx \frac{12\eta L\alpha}{h^4}\frac{1}{(1 - 0.63\alpha)}, \qquad \text{for} \ \alpha \to 0 \qquad (S4)$$

The effect of constriction width and length on the relative flow rates through outlet channels

Let us consider the cross-slot geometry used in hydrodynamic trapping (Fig. S2a). We would like to calculate (Q_c/Q_{tot}), the ratio of the flow rate through the outlet channel with the constriction (Q_c) to the total flow rate ($Q_{tot} = Q_c + Q_n$) as a function of the constriction width (w_c) and length (L_c). We assume that the flow is pressure-driven from a common source and the outlet channels

---

* To whom correspondence should be addressed: cms@illinois.edu.
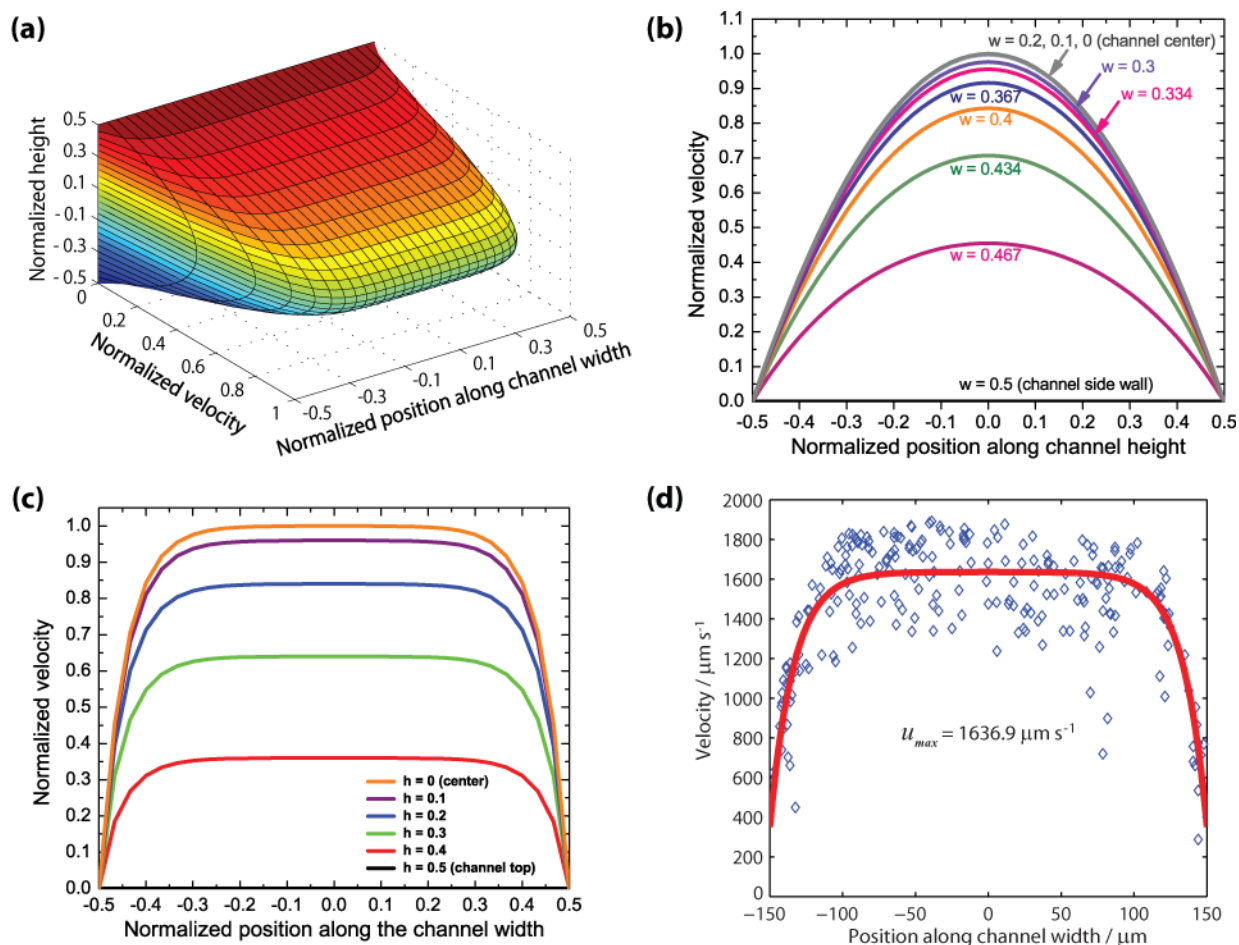
(a)

(b)

(c)

(d)

Fig. S1 Velocity Profile in a Rectangular Microchannel. (a) Velocity profile for laminar flow in a rectangular microchannel with aspect ratio of $\alpha = h/w = 0.166$. The axes are normalized to the channel width ($w = 300$ μm), the channel height ($h = 50$ μm) and the maximum velocity. (b) The velocity profile along the channel height is parabolic with increasing maximum velocity towards the centre of the channel along the channel height. (c) For low aspect ratios, the flow in rectangular microchannels is plug-like flow and the global maximum velocity is attained at a distance (0.2×channel width) from the channel walls along the channel width. (d) The experimental velocity profile along the channel width is obtained by tracking and measuring the velocity of individual fluorescent beads flowing in the microchannel at half height. From the fit to the experimental data, the maximum velocity in the microchannel is obtained to calculate the flow rates in Fig. 5 in the main text.

open to atmospheric pressure. In this case, the pressure drop across both outlet channels is the same and the outlet channels are analogous to resistors connected in parallel. As a result, the flow rate through the outlet channel with the constriction is proportional to the flow resistance of the opposite channel:

$$\frac{Q_c}{Q_{tot}} = \frac{R_n}{R_{tot}} = \frac{R_n}{R_n + R_c} = \frac{1}{1 + \frac{R_c}{R_n}} \qquad (S5)$$

We can obtain an expression for (Q_c/Q_{tot}) using the approximate flow resistance formula in Eq. (S4) where R_n and R_c are given by:

$$R_n \approx \frac{12\eta L\alpha}{h^4} \frac{1}{(1 - 0.63\alpha)} \quad \text{and} \quad R_c \approx \frac{12\eta L\alpha}{h^4}\left(\frac{1 - \gamma_{lc}}{1 - 0.63\alpha} + \frac{\gamma_{lc}}{\gamma_{wc} - 0.63\alpha}\right), \quad \text{for } \alpha \to 0 \qquad (S6)$$

where $\gamma_{wc} = w_c/w$ and $\gamma_{lc} = L_c/L$ are the normalized constriction width and length respectively. Combining Eq. (S5) and (S6), we obtain (Q_c/Q_{tot}) as a function of γ_{wc} and γ_{lc}:

$$\frac{Q_c}{Q_{tot}}[\gamma_{wc}, \gamma_{lc}] = \frac{1}{2 + \gamma_{lc}\left(\frac{1 - \gamma_{wc}}{\gamma_{wc} - 0.63\alpha}\right)} \qquad (S7)$$

As $\gamma_{wc} \to 1$ or $\gamma_{lc} \to 0$, the constriction vanishes and Eq. (S7) correctly predicts that the flow splits equally ($Q_c/Q_{tot} \to 1/2$).

2

Fig. S2 The effect of constriction width and length on the relative flow rates.
(a) The device layout for the one-constriction configuration. (b) For the device design illustrated in (a), Eq. (S2) (exact) and Eq. (S3) (approximation) are used to calculate the ratio of the flow rate through the outlet channel with the constriction (Q_c) to the total flow rate (Q_{tot}) as a function of normalized constriction width (γ_{wc}) and length (γ_{lc}). Eq. (S3) is a good approximation to Eq. (S2), however it deviates from the exact solution for $\gamma_{wc} < 0.2$ corresponding to an aspect ratio of approximately $\alpha_c \geq 1$ for the constriction. For $\gamma_{wc} = 1$, the constriction vanishes and the flow is split equally ($Q_c = Q_n$). (Inset) The outlet channel flow resistance increases almost linearly with the constriction length (γ_{lc}) leading to a linear decrease in (Q_c/Q_{tot}). The constriction width (w_c) and length (L_c) are normalized to the microchannel width ($w = 300$ μm) to obtain (γ_{wc}) and (γ_{lc}).
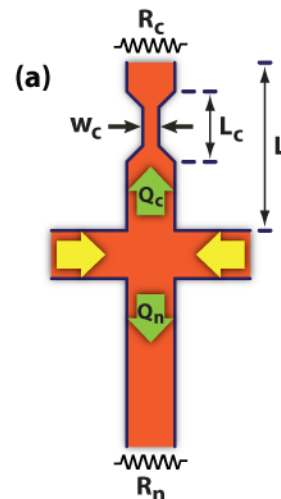

Fig. S2b shows the plot for (Q_c/Q_{tot}) as a function of normalized constriction width (γ_{wc}) using Eq. (S7) (see Approximation plot).

Eq. (S7) is a good approximation to (Q_c/Q_{tot}) for $\alpha < \gamma_{wc} < 1$, however it deviates from the exact solution for $\gamma_{wc} < \alpha$. As $\gamma_{wc} \to 0$, the flow resistance of the outlet channel with the constriction goes to infinity ($R_c \to \infty$); therefore the flow rate through this channel should approach to zero ($Q_c \to 0$, ∴ $Q_c/Q_{tot} \to 0$). Eq. (S7) does not predict this behaviour correctly as $\gamma_{wc} \to 0$, $R_c \to 1/(2 - \gamma_{lc}/0.63\alpha)$, which is also observed on the plot (approximation) in Fig. S2b for $\gamma_{wc} < 0.2$.

A more accurate result for (Q_c/Q_{tot}) can be obtained from Eq. (S5) using the "exact" flow resistances of the outlet channels rather than using the approximate formulas given in Eq. (S6). The "exact" flow resistances are derived from Eq. (S2):

$$R_n = \frac{12\eta L\alpha}{h^4}\left[1 - \sum_{n,odd}^{\infty}\frac{192\alpha}{(n\pi)^5}\tanh\left(\frac{n\pi}{2\alpha}\right)\right]^{-1} \qquad (S8)$$

$$R_c = R_n(1 - \gamma_{lc}) + R_{ctr} \qquad (S9)$$

where R_{ctr} is the flow resistance of the constriction given by:

$$R_{ctr} = \frac{12\eta L\alpha}{h^4}\left(\frac{\gamma_{lc}}{\gamma_{wc}}\right)\left[1 - \sum_{n,odd}^{\infty}\frac{192}{(n\pi)^5}\left(\frac{\alpha}{\gamma_{wc}}\right)\tanh\left(n\pi\frac{\gamma_{wc}}{2\alpha}\right)\right]^{-1} \qquad (S10)$$

The first 50 terms of the power series expansion are included in the calculation of the flow resistances. The resulting (Q_c/Q_{tot}) is plotted as a function of normalized constriction width (γ_{wc}) (see Exact plot) and length (γ_{lc}) (see inset plot). As expected, this solution produces a more accurate result and predicts correctly that as $\gamma_{wc} \to 0$, $Q_c/Q_{tot} \to 0$. For the device design depicted in Fig. S2a, we conclude that (Q_c/Q_{tot}) exhibits a sigmoidal and a linear decay response against changes in constriction width (w_c) and length (L_c) respectively.

Now, let us consider the device layout with a cross-slot geometry and two constrictions (one on each outlet channel) as illustrated in Fig. 5a in the main text. One constriction has a fixed width where the other has a variable width. We calculated (Q_v/Q_{tot}), the ratio of the flow rate through the outlet channel with the variable constriction (Q_v) to the total flow rate ($Q_{tot} = Q_c + Q_v$) as a function of the variable constriction width (w_v) and length (L_v). Similar to Eq. (S5), (Q_v/Q_{tot}) is given by:

$$\frac{Q_v}{Q_{tot}} = \frac{R_c}{R_{tot}} = \frac{R_c}{R_c + R_v} = \frac{1}{1 + \dfrac{R_v}{R_c}} \qquad (S11)$$

The flow resistance of the outlet channel with the fixed constriction (R_c) is given by Eqs. (S8-S10). The flow resistance of the outlet channel with the variable constriction (R_v) is given by:

$$R_v = R_n(1 - \gamma_{lv}) + R_{var} \quad \text{where} \quad R_{var} = \frac{12\eta L\alpha}{h^4}\left(\frac{\gamma_{lv}}{\gamma_{wv}}\right)\left[1 - \sum_{n,odd}^{\infty}\frac{192}{(n\pi)^5}\left(\frac{\alpha}{\gamma_{wv}}\right)\tanh\left(n\pi\frac{\gamma_{wv}}{2\alpha}\right)\right]^{-1} \qquad (S12)$$

3
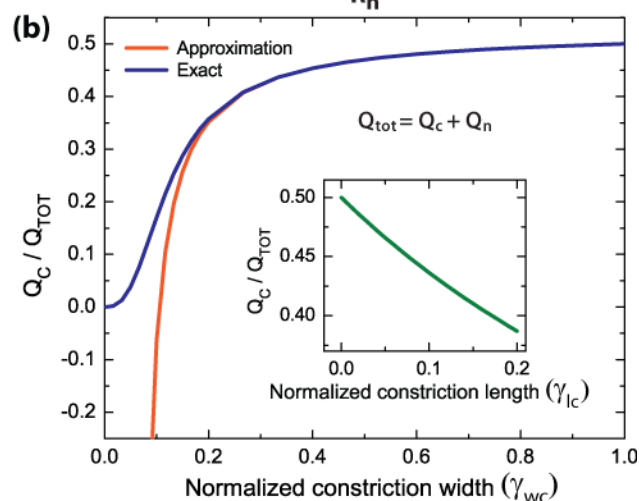
where $\gamma_{wv} = w_v/w$ and $\gamma_{lv} = L_v/L$ are the normalized width and length of the variable constriction respectively. R_{var} is the flow resistance of the variable constriction. In Fig. 5c, (Q_v/Q_{tot}) is plotted as a function of the normalized width of the variable constriction (γ_{wv}) (main plot, solid line) and length (γ_{lv}) (inset). Once more, we conclude that (Q_v/Q_{tot}) is sigmoidal for changes in the width of the variable constriction (w_v) and decreases almost linearly with changes in the length of the variable constriction (L_v).

The effect of constriction height on the relative flow rates through outlet channels

In the previous section, we assumed that the variable parameter for the constriction is its width. However, in our microfluidic trap, the membrane valve constricts the microchannel along the width *and* the height. Therefore, it would be useful to calculate the effect of constriction height on the flow resistance of the microchannel and on the relative flow rates through the outlet channels.

We again consider the device design in Fig. 5a with one fixed and one variable constriction. This time, for the variable constriction, we assume that the variable parameter is the height of the constriction rather than its width (Fig. 5b). We calculated (Q_v/Q_{tot}), the ratio of the flow rate through the outlet channel with the variable constriction (Q_v) to the total flow rate $(Q_{tot} = Q_c + Q_v)$ as a function of the variable constriction height (h_v). Once more, (Q_v/Q_{tot}) and the flow resistance of the outlet channel with the fixed constriction (R_c) is given by Eq. (S11) and Eqs. (S8-S10) respectively. However, the flow resistance of the outlet channel with the variable constriction (R_v) is given by:

$$R_v = R_n(1 - \gamma_{lv}) + R_{var} \quad \text{where} \quad R_{var} = \frac{12\eta L\alpha}{h^4}\left(\frac{\gamma_{lv}}{\gamma_{hv}{}^3}\right)\left[1 - \sum_{n,odd}^{\infty}\frac{192\alpha\gamma_{hv}}{(n\pi)^5}\tanh\left(\frac{n\pi}{2\alpha\gamma_{hv}}\right)\right]^{-1} \qquad (S13)$$

where $\gamma_{hv} = h_v/h$ is the normalized height of the variable constriction. Fig. 5c depicts (Q_v/Q_{tot}) plotted as a function of the normalized height of the variable constriction (γ_{hv}). The response of the relative flow rate (Q_v/Q_{tot}) against changes in the height of the variable constriction is also sigmoidal, however the shape of the response curve is different than the response curve for changing the constriction width. The relative flow rate response against changes in the constriction width and height are linear and sensitive between $0 < \gamma_{wv} < 0.2$ and $0.1 < \gamma_{hv} < 0.6$ respectively.

Experimental determination of the relative flow rates through outlet channels

For a pressure-driven, steady-state flow in a microchannel with a rectangular cross section, the fluid velocity averaged over the channel height is given by:

$$\bar{u}(y) = \frac{1}{h}\int_0^h dz\, \mathbf{u}(y,z) = \frac{8h^2\Delta p}{\pi^4\eta L}\sum_{n,odd}^{\infty}\frac{1}{n^4}\left[1 - \frac{\cosh\left(n\pi\frac{y}{h}\right)}{\cosh\left(n\pi\frac{w}{2h}\right)}\right] \qquad (S14)$$

At the middle of the channel $(y = 0)$ and at the channel wall $(y = w/2)$, the averaged fluid velocity yields:

$$\bar{u}(0) = \frac{h^2\Delta p}{12\eta L}\left[1 - \delta\right] \quad \text{where} \quad \delta = \sum_{n,odd}^{\infty}\frac{96}{(n\pi)^4\cosh\left(n\pi\frac{w}{2h}\right)} \quad \text{and} \quad \bar{u}(w/2) = 0 \qquad (S15)$$

The maximum fluid velocity in the channel occurs at the middle of the channel height and width:

$$u_{max} = \mathbf{u}(0, h/2) = \frac{h^2\Delta p}{8\eta L}[1 - \beta] \quad \text{where} \quad \beta = \sum_{n,odd}^{\infty}\frac{48\sin\left(\frac{n\pi}{2}\right)}{(n\pi)^3\cosh\left(n\pi\frac{w}{2h}\right)} \qquad (S16)$$

Now, let's consider a pressure-driven, steady-state flow between two infinite parallel plates seperated by the channel height (h). The averaged and maximum fluid velocity for this flow type are given by:

$$\bar{u}(0) = \frac{h^2\Delta p}{12\eta L} \quad \text{and} \quad u_{max} = \frac{3}{2}\bar{u}(0) = \frac{h^2\Delta p}{8\eta L} \qquad (S17)$$

Comparing Eqs. (S15) and (S16) with Eq. (S17), it is obvious that δ and β are correction terms specifying the deviation of the averaged and maximum fluid velocity in the rectangular microchannel from the fluid velocities between two infinite parallel plates. The correction terms for five different aspect ratios are provided in Table S1.

Table S1 reveals that as the aspect ratio approaches to zero, the correction terms also approach to zero. Therefore, as the aspect ratio tends to zero, the flow in rectangular microchannels is increasingly plug-like and can be approximated by pressure driven flow between two infinite parallel plates. As a result, for a rectangular microchannel with low aspect ratio ($\alpha \leq 0.166$), the averaged and

Table S1 Correction terms for the averaged and maximum fluid velocity in a rectangular microchannel.
We calculated the correction factors (δ) and (β) for five different aspect ratios.

Aspect ratio	Correction term (δ) for averaged velocity	Correction term (β) for maximum velocity
0.1	2.97E-07	4.67E-07
0.166	0.00016	0.00025
0.333	0.0177	0.0278
0.5	0.085	0.134
1	0.393	0.616

maximum fluid velocities are estimated by Eq. (S17) with < 0.03 % accuracy. In this case, following Eq. (S3), the volumetric flow rate (Q) in the microchannel is given by:

$$Q \approx \frac{h^3 w \Delta p}{12 \eta L}(1 - 0.63\alpha) = \bar{u}A(1 - 0.63\alpha) = \frac{2}{3}u_{max}A(1 - 0.63\alpha) \quad \text{for } \alpha \to 0 \qquad \text{(S18)}$$

where $A = hw$ is the cross-sectional area of the microchannel. Eq. (S18) indicates that the flow rate is proportional to the maximum velocity in the microchannel. Hence, to calculate the relative flow rates through the outlet channels, the maximum velocity in each outlet channel can be used as a measure of the flow rate. For instance, (Q_v/Q_{tot}) for the device in Fig. 5a (main text) yields:

$$\frac{Q_v}{Q_{tot}} = \frac{(u_{max})_v}{(u_{max})_c + (u_{max})_v} \qquad \text{(S19)}$$

where $(u_{max})_c$ and $(u_{max})_v$ are the maximum fluid velocities in the outlet channels with a fixed and variable constriction size respectively. To determine the maximum fluid velocities in the outlet channels, a dilute fluorescent bead solution is introduced to each microfluidic trapping device and individual beads are tracked while flowing through the outlet channels. For each outlet channel, the experimental velocity profile across the channel width is plotted by measuring the position and velocity of individual beads flowing through at half channel height (Fig. S1d). The maximum fluid velocity in each outlet channel is obtained by fitting the experimental velocity profile to the theoretical velocity profile at the middle of the channel height, $u(y, h/2)$:

$$u\left(y, \frac{h}{2}\right) = \frac{4h^2 \Delta p}{\pi^3 \eta L} \sum_{n,odd}^{\infty} \frac{1}{n^3}\left[1 - \frac{\cosh\left(n\pi \frac{y}{h}\right)}{\cosh\left(n\pi \frac{w}{2h}\right)}\right]\sin\left(\frac{n\pi}{2}\right) \qquad \text{(S20)}$$

The first term in the power series expansion is used as the functional form to perform the fit yielding only 3.2% error. The relative flow rates through the outlet channels are calculated by Eq. (S19) using the maximum fluid velocity obtained from the fit for each outlet channel.

Table S2 Experimental values of relative flow rates through the outlet channels (Q_v/Q_{tot}) from Figure 5c.
The flow partitioning function (Q_v/Q_{tot}) is experimentally measured for seven different variable constriction widths to determine the effect of valve cross-sectional area on the relative flow rates through the outlet channels.

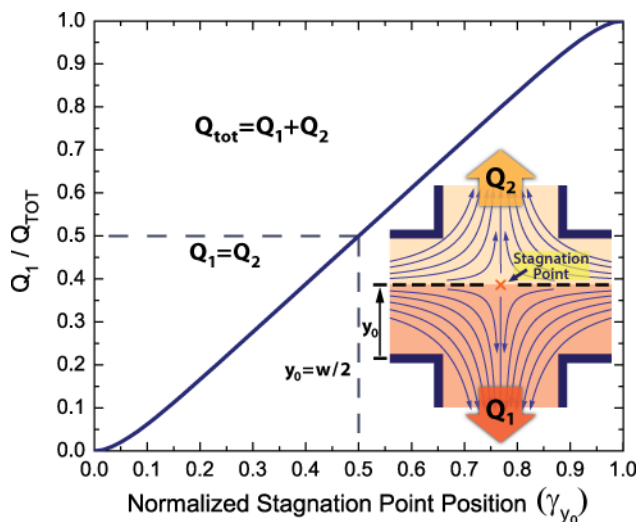| Normalized variable constriction width	Relative flow rates (Qv/Qtot)
0.133	0.232 ± 0.010
0.2	0.388 ± 0.017
0.333	0.484 ± 0.019
0.466	0.508 ± 0.020
0.6	0.529 ± 0.022
0.666	0.532 ± 0.021
0.866	0.562 ± 0.022

Fig. S3 The effect of the stagnation point position on the relative flow rates. We calculated the ratio of the flow rate through one of the outlet channels to the total flow rate as a function of stagnation point position. Due to the plug-like velocity profile in the microchannels (see Fig. S1c), (Q_1/Q_{tot}) is linear with the stagnation point position and only deviates from linearity as the stagnation point position approaches the channel walls. When the stagnation point position is at the middle of the channel ($y_0 = w/2$), the flow is split equally ($Q_1 = Q_2$). The stagnation point position is then normalized to the microchannel width (w).

The effect of the stagnation point position on the relative flow rates through outlet channels

Let us consider the effect of the stagnation point position on the ratio of the flow rate through one of the outlet channels (Q_1) to the total flow rate ($Q_{tot} = Q_1 + Q_2$) (Fig. S3). The incoming flow splits into two (shown by two different colors) along the axis passing through the stagnation point and parallel to the inlet channels. The flow rates through the two outlet channels can be given by:

$$Q_1 = \int_{-w/2}^{y_0} dy \int_0^h dz\, u(y,z) \quad \text{and} \quad Q_2 = \int_{y_0}^{w/2} dy \int_0^h dz\, u(y,z) \qquad (S21)$$
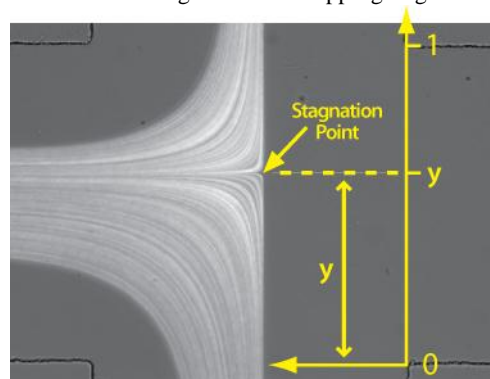
Combining Eq. (S1) and (S21), we get:

$$\frac{Q_1}{Q_{tot}}[\gamma_{Y0}] = \frac{\gamma_{Y0} + \frac{1}{2}\left(1 - \sum_{n,odd}^{\infty}\frac{192\alpha}{(n\pi)^5}\left[\frac{\sinh\left(n\pi\frac{\gamma_{Y0}}{\alpha}\right)}{\cosh\left(\frac{n\pi}{2\alpha}\right)} + \tanh\left(\frac{n\pi}{2\alpha}\right)\right]\right)}{\left(1 - \sum_{n,odd}^{\infty}\frac{192\alpha}{(n\pi)^5}\tanh\left(\frac{n\pi}{2\alpha}\right)\right)} \qquad (S22)$$

where $\gamma_{Y0} = y_0/w$ is the normalized stagnation point position. If ($\gamma_{Y0} \to -1/2$), there is no flow going through outlet 1 and ($Q_1/Q_{tot} \to 0$). When the stagnation point is at the center ($\gamma_{Y0} = 0$), the flow splits equally and ($Q_1/Q_{tot} = 1/2$). As ($\gamma_{Y0} \to 1/2$), there is no flow going through outlet 2 and therefore ($Q_1/Q_{tot} \to 1$). Fig. S3 shows the plot for (Q_1/Q_{tot}) as a function of the normalized stagnation point position ($0 < \gamma_{Y0} < 1$) using Eq. (S22). The coordinate axis for the stagnation point position (γ_{Y0}) is translated by half a channel width ($-w/2 < y_0 < w/2 \to 0 < y_0 < w$) and normalized to the channel width (w). As can be seen from Fig. S3, the incoming flow splits linearly with the stagnation point position which has a major implication on the design of the hydrodynamic trap as described in the main text.

Experimental determination of the stagnation point position

The stagnation point position data for various variable constriction widths illustrated in Fig. 6 (main text) are determined experimentally by fluorescent bead tracking. The position of the stagnation point is revealed by tracking the fluorescent beads passing through the trapping region. For this purpose, a sample stream containing 2.2 µm diameter fluorescent beads (nile red, 0.01 % w/v) is introduced to the stagnation point flow generated at the trapping region. Since the sample stream is flow-focused, the beads mainly pass through the vicinity of the stagnation point which is located nearby the center of the microchannel junction. 600 consecutive images of the trapping region are captured and recorded by a fluorescence microscope and a CCD camera. The successive images are then overlaid to reveal the stagnation point (Fig. S4). The position of the stagnation point is determined visually with one pixel accuracy which corresponds to 1 µm with our current microscopy setup (10x magnification and a CCD camera with 9.9 µm pixel size). The stagnation point position is then normalized to the channel width determined experimentally for each device used in collecting data for Fig. 6.

Fig. S4 Determining the Stagnation Point Position. The stagnation point position is obtained via the images of fluorescent beads flowing through the trapping region (microchannel junction). 600 successive images are overlaid to reveal the stagnation point and determine its position with one pixel accuracy corresponding to 1 µm. The stagnation point position is normalized to the microchannel width.

References

1. H. Bruus, *Theoretical microfluidics*, Oxford University Press, Oxford ; New York, 2008.